JOURNAL OF COLLOID AND INTERFACE SCIENCE **187,** 313–326 (1997)
ARTICLE NO. CS964702

Nonlinear Dynamics of Lipid Films under Electric Forces

E. RAMOS-DE-SOUZA,*,† C. ANTENEODO,* N. M. COSTA-PINTO,‡ AND P. M. BISCH[1,]*

*Instituto de Biofísica Carlos Chagas Filho, UFRJ, CCS, sala G026, Cidade Universitária, Ilha do Fundão, 21949-900, Rio de Janeiro, RJ, Brazil;
†Centro Federal de Educação Tecnológica da Bahia, Rua Emidio Santos, s/n, Barbalho, 40300-100, Salvador, BA, Brazil;
and ‡Instituto de Física, UFBA, Campus Universitário da Federação, 40000-000, Salvador, BA, Brazil

Received March 19, 1996; accepted November 19, 1996

We study the dynamics and rupture of lipid films perturbed in the symmetric mode squeezing through an electrohydrodynamical approach. The lipid phase and the two surrounding aqueous phases are considered as incompressible Newtonian viscous fluids submitted to van der Waals, steric, and electric body forces. A nonlinear evolution equation for the film thickness, at the long-wavelength limit, is obtained for two symmetric cases: a film with equally charged surfaces with no potential drop and a neutral film submitted to an external electric field. At the long-wavelength limit, the electric term only influences the film evolution when the electric field inside the film is nonvanishing. We solve numerically, as an initial value problem with periodic boundary conditions, the nonlinear evolution equation. The rupture time is obtained and compared with analytical estimates. Sufficiently strong steric forces prevent the film from narrowing beyond a minimum thickness leading the film to a steady state different from the planar one consistently with the nonlinear analytical approach. The presence of a transmembrane electric potential destabilizes the perturbed film as predicted by the linear and nonlinear approaches; however, as expected, destabilization is not relevant at physiological values of the potential drop.

Key Words: **lipid bilayer; film stability; transmembrane electric potential.**

1. INTRODUCTION

The lipid bilayer, composed of two lipidic monolayers, where proteins are embedded, constitutes the basic structure of biological membranes (1). Under normal physiological conditions, this structure reaches a stable equilibrium due to the stabilizing interactions of the hydrocarbon chains inside the bilayer, whereas in some nonequilibrium situations, the structure may break. Many cellular phenomena are associated with the movements, deformation, and rupture of biomembranes, e.g., endocytosis, exocytosis, and cell division. These phenomena take place when perturbations of the membrane environment generate interfacial instabilities (2). We study here the instability of the squeezing (SQ) mode where rupture may occur.

The formalism for describing the time evolution of the surfaces of an aqueous film perturbed in the SQ mode and subject to van der Waals body forces was detailed in a previous work (3). In the present work, we recall that formalism to model a lipid film submitted to van der Waals, steric, and electric body forces. Basically, a general nonlinear evolution equation, valid in the long-wavelength limit, was derived from the Navier–Stokes equation, considering the lipidic and external phases as incompressible Newtonian viscous fluids. The equation is fully expressed in terms of the film thickness for the particular case of a film with tangentially immobile surfaces. The electrohydrodynamical approach takes into account that the lipid molecules that compose the film are submitted to attractive van der Waals forces, repulsive steric forces due to the overlap of the hydrocarbon chains of the lipid molecules, and electrical Coulombic forces. The latter arise from the presence of charges both at the surface of the film, since lipid head groups may have a net electric charge, and in the external environment, normally an aqueous electrolyte solution. External electric fields may be also present. Two symmetric cases are considered: a film with equally charged surfaces (case I) and a neutral film submitted to a potential drop (case II).

Estimates of the rupture time are obtained analytically through linear and nonlinear approximations. The former consists of linearizing the evolution equation around a planar state; then, the linearized equation admits solutions in normal modes, while the nonlinear approach is based on the perturbative method proposed by Sharma and Ruckenstein (4–6) that linearizes the evolution equation around a nonuniform stationary state. These treatments provide a good qualitative idea about the influence of the physical parameters that characterize the system both on rupture times and on ranges of wavenumbers for stability. Although the second perturbative method preserves some finite-amplitude nonlinear effects, both approaches apply to situations where the disturbance amplitude is small compared with the film thickness, and therefore, they fail as the perturbation grows to

[1] To whom correspondence should be addressed.

0021-9797/97 $25.00

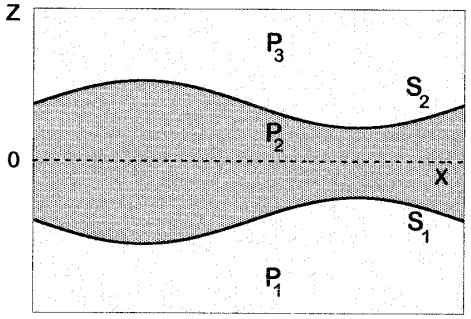

FIG. 1. Film model. Three bulk phases P_1, P_2, and P_3 separated by two surfaces S_1 and S_2. The deformed film phase P_2 is represented in the SQ mode where the displacements of the film surfaces are 180°C out of phase.

amplitudes of the order of film thickness, precisely the situation close to rupture.

Alternatively, the numerical solution of the film evolution equation, also obtained in the present work, allows us to follow the complete dynamics of the film up to rupture, whenever concomitant, thus giving a better estimation of the rupture time. Also, the film may reach a nonplanar steady state and rupture does not occur. In both cases, numerical results are qualitatively consistent with those from the nonlinear analytical approach.

2. ELECTROHYDRODYNAMIC MODEL

We consider three bulk phases P_1, P_2, and P_3 separated by two surfaces S_1 and S_2 (Fig. 1). The film is represented by the inner thin bulk phase P_2 of mass density ρ, viscosity μ, and dielectric constant ϵ, limited by two interfaces with identical surface tension Σ. The external bulk phases P_1 and P_3 consist of identical aqueous electrolytic phases with mass density ρ', viscosity μ', and dielectric constant ϵ'. The surfaces are considered two-dimensional material ones, located at $z = \pm h(x, t)/2$, where h is the film thickness that depends on both lateral coordinate x and time t.

The film is submitted to long-range van der Waals forces, electric coulombic forces due to electrical double-layers (7, 8) in the external bulk phases, and steric forces due to the overlap of the hydrocarbon chains in the film phase (8). These interactions are taken as body forces in an electrohydrodynamical approach and the three bulk phases are treated as incompressible Newtonian viscous fluids. The movement of a volume element in each bulk phase obeys the Navier–Stokes equation in the form

$$\rho \frac{d\mathbf{V}}{dt} = \nabla \cdot \underline{\mathbf{P}} + \nabla \cdot (\underline{\mathbf{T}} + \underline{\mathbf{\Pi}}) - \rho \nabla W \qquad [1]$$

and the incompressibility condition reads

$$\nabla \cdot \mathbf{V} = 0, \qquad [2]$$

where the vector $\mathbf{V}$ represents the velocity field. In Eq. [1], $\underline{\mathbf{P}}$, $\underline{\mathbf{\Pi}}$, and W are, respectively, the mechanical stress tensor, the steric stress tensor, and the van der Waals potential. We considered the steric tensor proposed in a semiphenomenological approach (8) that describes the steric forces in the lipid phase. The van der Waals potential is assumed to have the form adopted by William and Davies (3). $\underline{\mathbf{T}}$ is the Maxwell stress tensor given in the form

$$\underline{\mathbf{T}} = \frac{1}{4\pi}\left(\epsilon \mathbf{E}\mathbf{E} - \frac{1}{2} E^2 \underline{\mathbf{I}}\right), \qquad [3]$$

where $\mathbf{E}$ is the electric field, which describes the electrostatic interactions due to both external applied electric fields and surface charge densities.

We treat the three bulk phases as isotropic, homogeneous, and linear electrical media. In this way, in the internal phase a scalar electric potential ψ satisfies the Laplace equation

$$\nabla^2 \psi = 0, \qquad [4]$$

as there is no excess of charge inside the film. In the external bulk phases, there occurs a spatial distribution of charges due to competition between the thermal and electrostatic energies of the ions. We consider ion diffusion large enough to recover the Boltzmann distribution as the film surfaces move, in such a way that the electrochemical potential in the aqueous phases remains constant. Then, the electrostatic potential ψ' at the external phases satisfies the Poisson–Boltzmann equation (7, 8)

$$\nabla^2 \psi' = \frac{8\pi Z_0 C_0}{\epsilon} \sinh\left(\frac{Z_0 \psi'}{RT}\right), \qquad [5]$$

where Z_0 is the electrolytic molar charge, C_0 is the ionic molar concentration at the external phases far away from the interfaces, R is the universal gas constant, and T is the absolute temperature.

Both movement and field equations are supplemented by suitable boundary conditions at the interfaces, which are considered as discontinuity surfaces with intrinsic rheological properties. We consider equilibrium of interfacial forces such that an intrinsic momentum source γ (for nonviscous interfaces) plus the jump of the stress tensor across the interfaces vanishes (9)

$$\gamma + \| - \underline{\mathbf{P}} + \underline{\mathbf{T}} + \underline{\mathbf{\Pi}} \| \cdot \mathbf{n} = 0. \qquad [6]$$

The jump of the electric displacement across the interfaces is proportional to the surface charge density σ_s,

$$\|\epsilon \mathbf{E}\| = 4\pi\sigma_s, \qquad [7]$$

while the electric potential is taken as continuous across the interfaces,

$$\|\psi\| = 0. \quad [8]$$

Since the interfaces are located at $z = \pm h(x, t)/2$, the spatiotemporal evolution of the free surfaces is described by the kinematic equation

$$v = \pm(h_t + uh_x)/2. \quad [9]$$

Inserting the solutions of the governing equations of the fluid in the kinematic equation [9] we obtain the spatiotemporal evolution of the film thickness (see Appendix),

$$H_\tau + \frac{1}{4}\left[H^3 H_{XXX} + H^{-1}H_X - P\,\frac{\sinh(\beta H/2)}{\cosh^3(\beta H/2)}\,H^3 H_X + q\left(\frac{\alpha H}{1+\alpha H}\right)^3 H_X\right]_X = 0, \quad [10]$$

where H is the adimensional thickness, X and τ are the rescaled adimensional spatial and time variables, respectively, and parameters P and β are related to steric forces while q and α are related to electric ones, as defined in the Appendix. Note that Eq. [10] was derived for case II; however, case I can also be obtained from Eq. [10] when $q = 0$. Equation [10] can be rewritten in the form

$$H_\tau + \tfrac{1}{4}[H^3[H_{XX} + \Pi(H)]_X]_X = 0, \quad [11]$$

where $\Pi(H)$ is the disjoining pressure (10). Here $\Pi(H)$ is given by

$$\Pi(H) = -\frac{1}{3}H^{-3} + \frac{P}{\beta\cosh^2(\beta H/2)} - \frac{q}{2}\left(\frac{\alpha}{1+\alpha H}\right)^2 \quad [12]$$

and will provide either film rupture or a nonplanar steady state depending on the film parameters (11).

3. APPROXIMATE ANALYTICAL SOLUTIONS

3.1. Linear Analysis

Equation [10] is a nonlinear partial differential equation. As it governs finite perturbations of the film surfaces, it also governs infinitesimal ones. In this section, we employ a linear stability analysis to obtain the first information about the dynamics of the system. We take $H = 1 + \mathcal{H}$ in Eq. [10], where $\mathcal{H} = \mathcal{H}(X, \tau)$ is a nondimensional infinitesimal quantity, and linearize in $\mathcal{H}$ to obtain

$$\mathcal{H}_\tau + \frac{1}{4}\left[\mathcal{H}_{XXXX} + \mathcal{H}_{XX} - p\mathcal{H}_{XX} + q\left(\frac{\alpha}{1+\alpha}\right)^3 \mathcal{H}_{XX}\right] = 0, \quad [13]$$

where $p = 4P\exp(-\beta)$ and we have taken $\beta \gg 1$. We assume a solution in normal modes for $\mathcal{H}(X, \tau)$ as

$$\mathcal{H}(X, \tau) = B_0 \exp(ikX + \omega_1 \tau), \quad [14]$$

where the nondimensional quantities B_0, k, and ω_1 are, respectively, the initial amplitude, wavenumber, and growth rate of the perturbation. Then, the dispersion equation reads

$$\omega_1 = -\frac{k^2}{4}[k^2 - k_{1c}^2], \quad [15]$$

where k_{1c} is the cutoff wavenumber verifying $\omega_1 = 0$ (marginal stability state) and is given by

$$k_{1c} = \left[1 - p + q\left(\frac{\alpha}{1+\alpha}\right)^3\right]^{1/2}. \quad [16]$$

It is easy to show that the perturbation grows for $0 < k < k_{1c}$. In this region the dispersion relation has a maximum at the dominant wavenumber k_{1m}

$$k_{1m} = k_{1c}/\sqrt{2}, \quad [17]$$

which satisfies $d\omega/dk = 0$, and the corresponding fastest rate of growth is

$$\omega_{1m} = \tfrac{1}{4}k_{1m}^2. \quad [18]$$

The growth rate, the cutoff wavenumber, the fastest rate of growth, and the dominant wavenumber are independent of the amplitude of the perturbation. If the transmembrane potential is negligible, we recover the results obtained for a neutral lipid film without electrical constraints (12) that corresponds to case I. Moreover, if the steric parameters are negligible, we recover the results for a neutral aqueous film (3). The linear analysis does not allow us to obtain the correct rupture time. Nevertheless, we estimate the linear rupture time τ_1 as the time necessary for the film surfaces to collapse ($H = 0$). Thus, taking the perturbation in the form given by Eq. [14], the linear rupture time is

$$\tau_l = -\frac{1}{\omega_{lm}} \ln B_0. \quad [19]$$

From Eqs. [15] to [17], it follows that while steric forces play a stabilizing role, electrostatic ones contribute to film destabilization. The cutoff wavenumber and the fastest rate of growth increase for larger values of the transmembrane potential. Therefore, a neutral film submitted to a potential drop, case II, is more unstable than a symmetric film with equally charged surfaces, case I. Note, from Eq. [19], that the linear rupture time τ_l decreases as the initial amplitude of the perturbation B_0 increases. Also, the maximal growth rate ω_{lm} may be interpreted as the inverse of the rupture time; then, both van der Waals and electric forces accelerate film rupture while the rupture time decreases due to steric forces.

3.2. Nonlinear Analysis

We perform a nonlinear analysis following the perturbative method proposed by Sharma and Ruckenstein (4–6) where the nonlinear evolution equation is linearized around a nonuniform stationary state. In this way, some nonlinearities are preserved. We consider that the total initial amplitude of the perturbation is expressed as $B_0 = \Delta + \delta$, where Δ and δ are the amplitudes of the reference stationary state and the time evolving part of the disturbance, respectively. In this way, we obtain the nonlinear dispersion relation

$$\omega_n = -\tfrac{1}{4}(1-\Delta)^3(k^2 - k_{nc^-}^2)(k^2 - k_{nc^+}^2), \quad [20]$$

where the subindex c applies to critical wavenumbers, verifying $\omega_n = 0$, and is given by

$$k_{nc^\pm} = X\sqrt{\left(1 \pm \sqrt{1 - \frac{4Y}{(1-\Delta)^3 X^4}}\right)\Big/ 2}, \quad [21]$$

with

$$Y = -\Delta(1-\Delta)^2 k_{lc}^2 (3k_{lc}^2 + (1-\Delta)^{-4} - 3q\alpha^3(1+\alpha(1-\Delta))^{-4} + P\left\{3\frac{\sinh(\beta(1-\Delta)/2)}{\cosh^3(\beta(1-\Delta)/2)} + \beta(1-\Delta)\frac{1/2 - \sinh(\beta(1-\Delta)/2)}{\cosh^4(\beta(1-\Delta)/2)}\right\}\right)$$

and

$$X = \sqrt{(1-\Delta)^{-4} - P\frac{\sinh(\beta(1-\Delta)/2)}{\cosh^3(\beta(1-\Delta)/2)} + q\left(\frac{\alpha}{1+\alpha(1-\Delta)}\right)^3}.$$

Indexes l and n are used for identifying linear and nonlinear quantities, respectively.

The dominant wavenumber is

$$k_{nm} = \frac{k_{nc^+}}{\sqrt{2}}\sqrt{1 + \frac{Y}{(1-\Delta)^3 k_{nc^+}^4}}. \quad [22]$$

Finally, the rupture time derived from the nonlinear approximation is

$$\tau_n = -\frac{1}{\omega_{nm}} \ln \frac{\delta}{1-\Delta}, \quad [23]$$

where $\omega_{nm} = \omega_n(k_{nm})$ is the fastest growth rate and may be written as

$$\omega_{nm} = \frac{1}{16}(1-\Delta)^3\left(1 - \frac{Y}{(1-\Delta)^3 k_{nc^+}^4}\right)^2 k_{nc^+}^4. \quad [24]$$

Note that linear results are recovered in the limit $\Delta \to 0$.

Depending on the disturbance wavelength, for fixed parameters of the attractive and repulsive interactions, different stability regimes are observed. The range of stable wavelengths may be inferred from the dispersion relation; the critical wavenumber k_c yielding $\omega(k_c) = 0$ determines the domains of stability. Following Eq. [15] (or Eq. [20] for $\Delta = 0$), the linear analysis predicts three regimes: if the disturbance wavenumber is $k > k_{lc}$, the perturbation vanishes and the film goes back to the planar steady state; if $k < k_{lc}$, the perturbation grows until the film breaks and, in the marginal case $k = k_{lc}$, the perturbation remains stationary.

Let us analyze now the more general dispersion equation [20]. A diagram of the nonlinear growth rate ω_n as a function of the wavenumber k and the amplitude of the reference stationary state Δ for the more simple case where steric and electric interactions are absent was obtained from Eq. [20] and is presented in Fig. 2a. The linear growth rate ω_l is recovered when $\Delta = 0$. The nonlinear method indicates that, as the initial amplitude increases, both the range of unstable wavenumbers stretches and the perturbation grows faster, then, the film becomes more unstable. We will adopt values for the film parameters considering reasonable ranges of known characteristic parameters for lipid films (8, 12–25). For $\mu = 1$ P, $\mu' = 10^{-2}$ P, $\rho = 1$ g/cm^3, $\rho' = 1$ g/cm^3, $\Sigma = 5$ dyn/cm, $A = 10^{-13}$ erg, $h_0 = 6 \times 10^{-7}$ cm, $\frac{1}{2}A_{\beta'}\beta'^2\eta_s^2 = 10^{14}$ dyn/cm^2, $\beta'^{-1} = 2.6 \times 10^{-8}$ cm, $\epsilon = 2.1$, $\epsilon' = 82$, $C_0 = 10$ mM, $T = 25$°C, and $\Delta\psi_T = -100$ mV, we have

$$P \approx 10^8, \quad p \approx 0.1, \quad q \approx 0.1, \quad \text{and} \quad \alpha \approx 40. \quad [25]$$

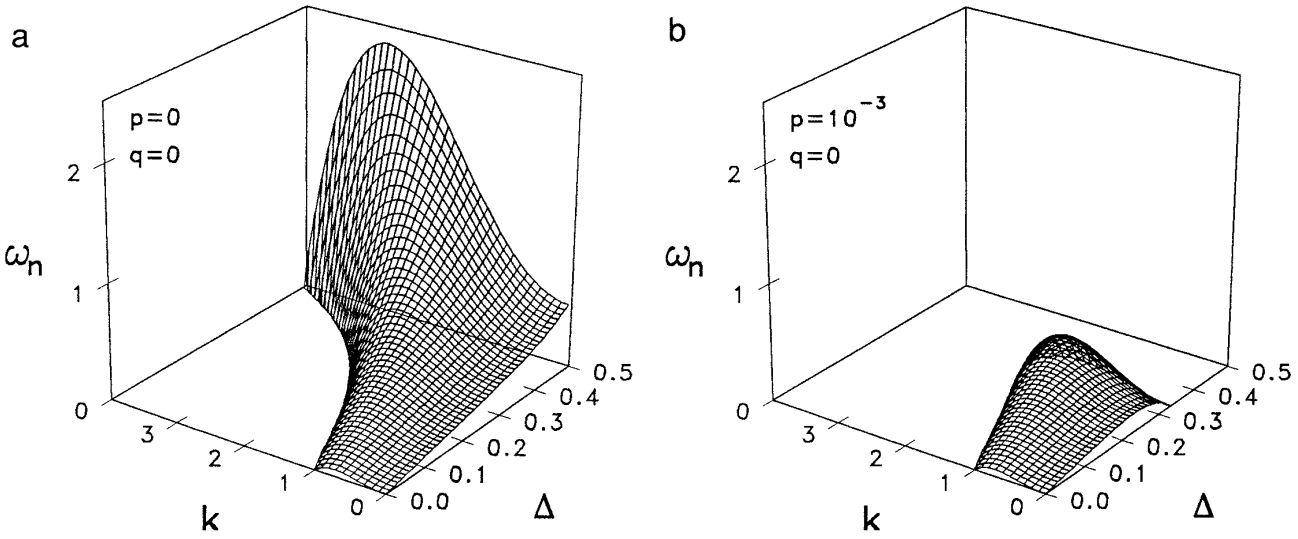

FIG. 2. Nonlinear growth rate ω_n as a function of the wavenumber k and the amplitude of the reference state Δ. Only positive values of ω_n, corresponding to the domains of instability, were plotted. (a) No steric nor electric forces. (b) Effect of steric forces with $\beta = 20$.

To analyze first the effect of steric forces on the stability diagram, electric forces will be neglected. A behavior qualitatively similar to the case $p = 0$ is observed for sufficiently small steric forces ($p \leqslant 10^{-4}$, when $\beta = 20$); i.e., the stability diagram is qualitatively the same as in Fig. 2a but the domain of stability is enlarged and maximal growth rates are reduced. The stabilizing role of these forces was already well known from the linear analysis (12); however, for larger values of the steric forces (Fig. 2b), nonlinearities become relevant and the domain of unstable wavenumbers is shrunk in such a way that the system may be prevented from reaching rupture.

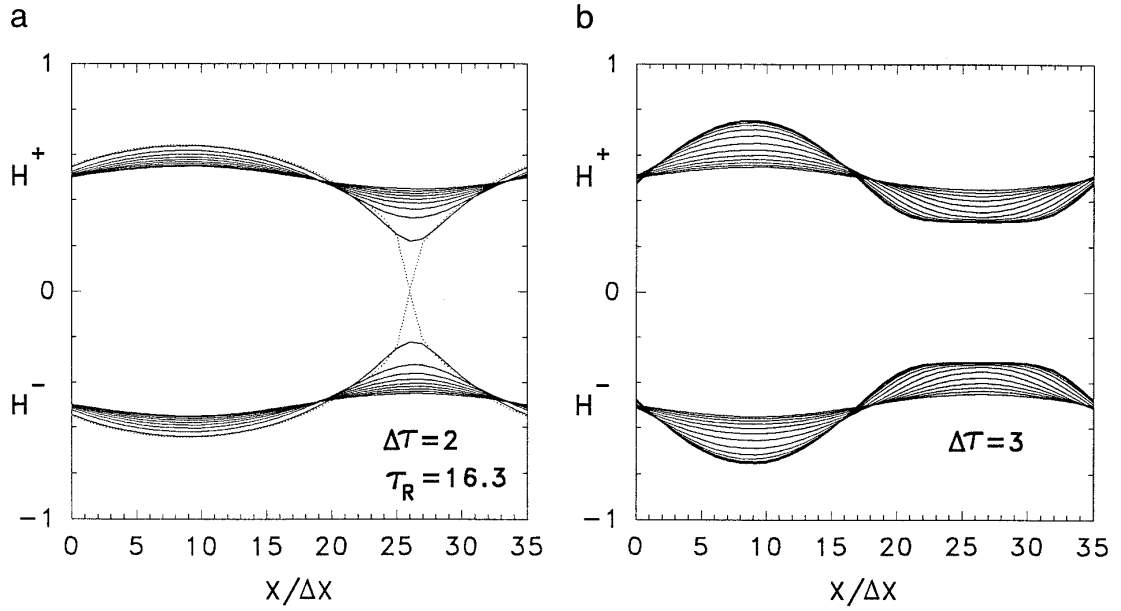

FIG. 3. Effect of steric forces on the evolution of the film. Film surfaces described by $H^{\pm}(X, \tau) = \pm H(X, \tau)/2$ as a function of $X/\Delta X$, where the dimensionless thickness H was obtained following the nonlinear Eq. [10] and $\Delta X = \lambda_m/35$. (a) Absence of either steric or electrostatic forces. (b) Presence of repulsive steric forces with $\beta = 20$ and $p = 10^{-2}$. In all cases, the perturbation with initial amplitude $B_0 = 0.1$ is in the k_m mode. Only one period of the periodic perturbation is represented. The curves represent the film surface shape at successive times distant by intervals $\Delta\tau$ as indicated in each figure, except for the dotted curves corresponding to the last time preceding rupture when concerned. The rupture time τ_R is indicated in (a). In (b), the film reaches a new steady state. Numerical integration was performed for time intervals $\delta\tau = 10^{-3}$ (a) and 5×10^{-4} (b).

As predicted by the linear approach, increasing values of the electrostatic parameter q lead the system to a more unstable situation. For typical values of q, a behavior qualitatively similar to that shown in Fig. 2a is observed but critical wavenumbers are shifted toward greater values and growth rates increased, i.e., an effect apparently opposite that of small steric forces; however, steric and electric nonlinear contributions to the dispersion relation are different and they affect the phase diagram in different ways.

4. NUMERICAL RESULTS

We follow basically the numerical methodology employed previously (3, 12). Equation [10] is solved as an initial value problem considering spatially periodic boundary conditions (PBC). This type of boundary conditions permits us to investigate the behavior of an ideal infinite film corresponding to the more realistic case of a film whose thickness is small compared with its length.

We consider initial values of the periodic form

$$H(X, 0) = 1 + B_0 \sin(kX).$$

Then, the bounded domain with PBC is $0 \leqslant X \leqslant 2\pi/k$. We note that, with this condition, the evolution is restricted to wavelengths being integer submultiples of $2\pi/k$.

We use finite-difference methods to solve Eq. [10], by means of a FTCS scheme (26). An explicit scheme is applied for the time derivative and centered staggered differences in space are used to obtain the successive derivatives with respect to X. Thereafter, the finite-difference representation of Eq. [10] is solved iteratively until $H(X, \tau) \leqslant 0$ for some X, after which the model loses applicability. Then, the numerical nonlinear rupture time τ_R is defined as the first time for which $H(X, \tau)$ vanishes at some point X.

To test the stability of the numerical scheme with respect to time and spatial grid we use a procedure previously described (3, 12) which basically consists of refining the grids within the limit set by the stability criteria (26). As a further test of reliability for the numerical method, we have verified that the integral of $H(X, \tau)$ over the period considered is conserved throughout the evolution.

By means of the numerical procedure described above, we are able to follow the evolution of the perturbed film. Since the perturbation is expected to rapidly tune the fastest growth mode, we follow the evolution of waves with wavenumber k_m where $k_m = k_{lm}$ is given by Eq. [17]; i.e., we follow the evolution of waves with the maximal growth rate given by the linear approximation. Results from numerical integration allow us to plot the shape of the film surfaces as a function of X at various times τ.

We analyzed the effect of the different forces on the evolution of the k_m mode. First we focused on steric effects by neglecting the electrostatic terms. As predicted by the stability analysis, for sufficiently small values of steric parameter p, the film perturbed in the k_m mode evolves up to rupture (similarly as in Fig. 3a, which corresponds to a film where steric and electric forces are negligible), even if steric forces have a stabilizing role which retards rupture, whereas for large values of p ($p \geqslant 10^{-4}$), a minimum thickness is allowed and the film reaches a steady state different from the marginal planar one (Fig. 3b). Through numerical integrations we observed that, for given values of the steric parameters, the same steady state is reached for any value of the initial amplitude of the disturbance. Figure 4 is a diagram outlining the evolution of the disturbance amplitude B in the presence of steric forces. Increasing parameter β has a similar effect as increasing p.

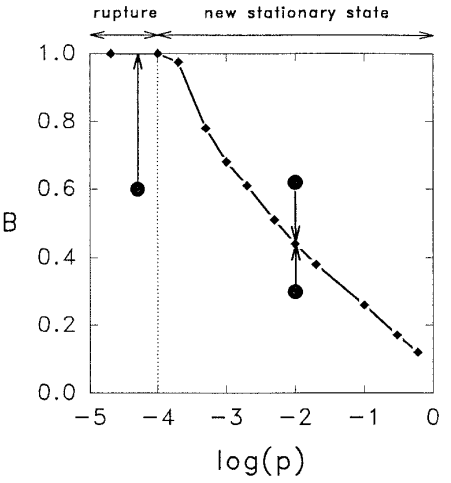

FIG. 4. Scheme of the time evolution of the disturbance amplitude B as a function of $\log p$, according to numerical results. The initial perturbation is in the k_m mode. The symbols (diamonds) correspond to values obtained from simulations by measuring the amplitude of the final steady state for some fixed p. Filled circles represent the initial condition and the arrows indicate the disturbance amplitude trajectory. Then, for sufficiently small p the film reaches rupture, whereas for $10^{-4} \leqslant p < 1$ the film cannot break for any initial amplitude, reaching a steady state different from the planar one. Note that, for $p = 1$, $k_m = k_c = 0$, then, for $p \geqslant 1$, any perturbation vanishes and the film goes to the planar state.

Electrostatic effects were also analyzed. The evolution of the film shape is qualitatively similar to the case where electrostatic forces are absent (Fig. 3a); it is the inner part of the wave that develops faster. The presence of a potential drop across the film, however, turns the film more unstable; i.e., the rupture time decreases, as anticipated by the analytical approaches. Increasing values of the electrostatic parameter q accelerate film rupture. The rupture time decreases almost exponentially with q (see Fig. 5a) and sigmoidally with α (Fig. 5b).

In Fig. 6, we follow the evolution of the velocity field inside the film using Eqs. [A22] and [A23], for the same conditions as in Figs. 3a and b. These diagrams allow us to

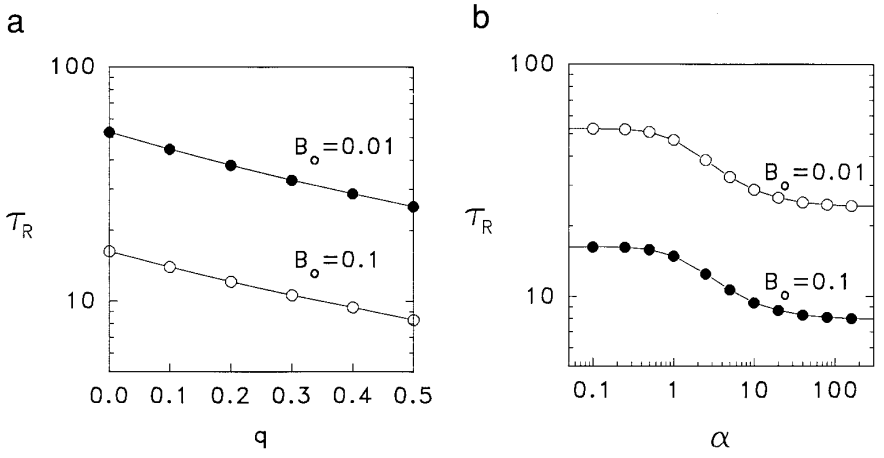

FIG. 5. Dependence of the rupture time τ_R on electrostatic parameters, for different values of the disturbance initial amplitude indicated in the figure. (a) τ_R vs q, with $\alpha = 40$. (b) τ_R vs α, with $q = 0.5$. Lines are guides to the eyes.

learn how fluxes originated. The symmetry properties derived from the SQ mode condition are verified: the tangential velocity u^0 is symmetric about $Z = 0$ vanishing at the film surfaces, whereas the normal velocity v^0 is antisymmetric about $Z = 0$. Also, the SQ mode condition imposes, at the center of the film, zero normal velocity, $v^0(Z = 0) = 0$, and no variation along the z axis of the tangential velocity, $u_Z^0(Z = 0) = 0$. In the case of Fig. 6a where steric and electric forces are absent we observe that, in the narrow regions of the film, flows are generated from the surface toward both the center and the broad regions. In the latter, fluxes are oriented toward the surface. Then, rupture arises from the flow of the fluid out from the region of initially small thickness where velocities increase more rapidly than in the broad regions. Electric forces and steric ones allowing rupture give place to velocity fields similar to those in Fig. 6a. The effect of steric forces large enough to prevent rupture is illustrated in Fig. 6b. Although not shown in the figure, further simulations show that flows tend to stop for sufficiently long times.

Figure 7 allows us to compare the values of the dimensionless rupture times obtained both by the numerical procedure and by the analytical linear and nonlinear approximations. Nonlinear rupture times were obtained assuming $B_0 = 2\Delta$ (i.e., $\delta = \Delta$), which seems to be the better choice. Figure 7 was obtained for the case where only electric forces are present, but it is qualitatively representative of the behavior of rupture times when light steric effects allowing rupture are present. The numerical rupture time τ_R decreases for increasing values of the initial amplitude of the perturbation, according to the predictions of the linear and nonlinear approximations; however, the analytical treatments overestimate rupture times. For disturbance amplitudes in the range 10^{-3} to 10^{-1}, the value of numerical rupture time is about 75% of that predicted through the analytical nonlinear approach. For increasing disturbance amplitude, the ratio between numerical and analytical rupture times decreases abruptly but the nonlinear ratio is higher, as expected.

We studied the evolution of a film perturbed in the squeezing mode. In all numerical integrations we followed the evolution of the film initially disturbed by single-mode sinoidal perturbations corresponding to the fastest growth mode according to the linear approximation. We could have also considered the nonlinear fastest growth mode instead of the linear one. Figure 8 shows the dependence of τ_R on the wavenumber k for the case $B_0 = 0.1$ when steric and electric forces are negligible. Note the flat shape of the numerically obtained plot around k_m. Therefore, in that case, there are no significant differences concerning rupture times whether we consider the linear or the nonlinear maximal wavenumber in the numerical integration. As nonlinearities increase, however, depending on the values of the initial amplitude and the parameters, that choice may lead to somewhat different results. For instance, for larger initial amplitudes, the plots in Fig. 8 would be more peaky around k_m. Nonlinear critical and maximal wavenumbers are dependent on the initial amplitude of the disturbance and, for a given value of the initial amplitude, nonlinearities normally shift the maximal wavenumber to greater values and growth rates are increased (see Fig. 2). This increase in instability will be reflected in the smaller rupture times resulting from the nonlinear approximation compared with the linear one (see Figs. 7 and 8).

In Fig. 9, we follow the evolution of a wave in the $k_m/2$ mode. If the perturbation amplitude is sufficiently small (Fig. 9a), the k_m mode is tuned before rupture; however, rupture occurs at the point of initially smaller thickness. For higher amplitudes (for instance, $B_0 = 0.1$, in Fig. 9b), the tendency to tune the k_m mode makes the outer part of the wave develop more slowly than in the k_m mode (Fig. 3a) and rupture is delayed but the film breaks before tuning the k_m mode. We

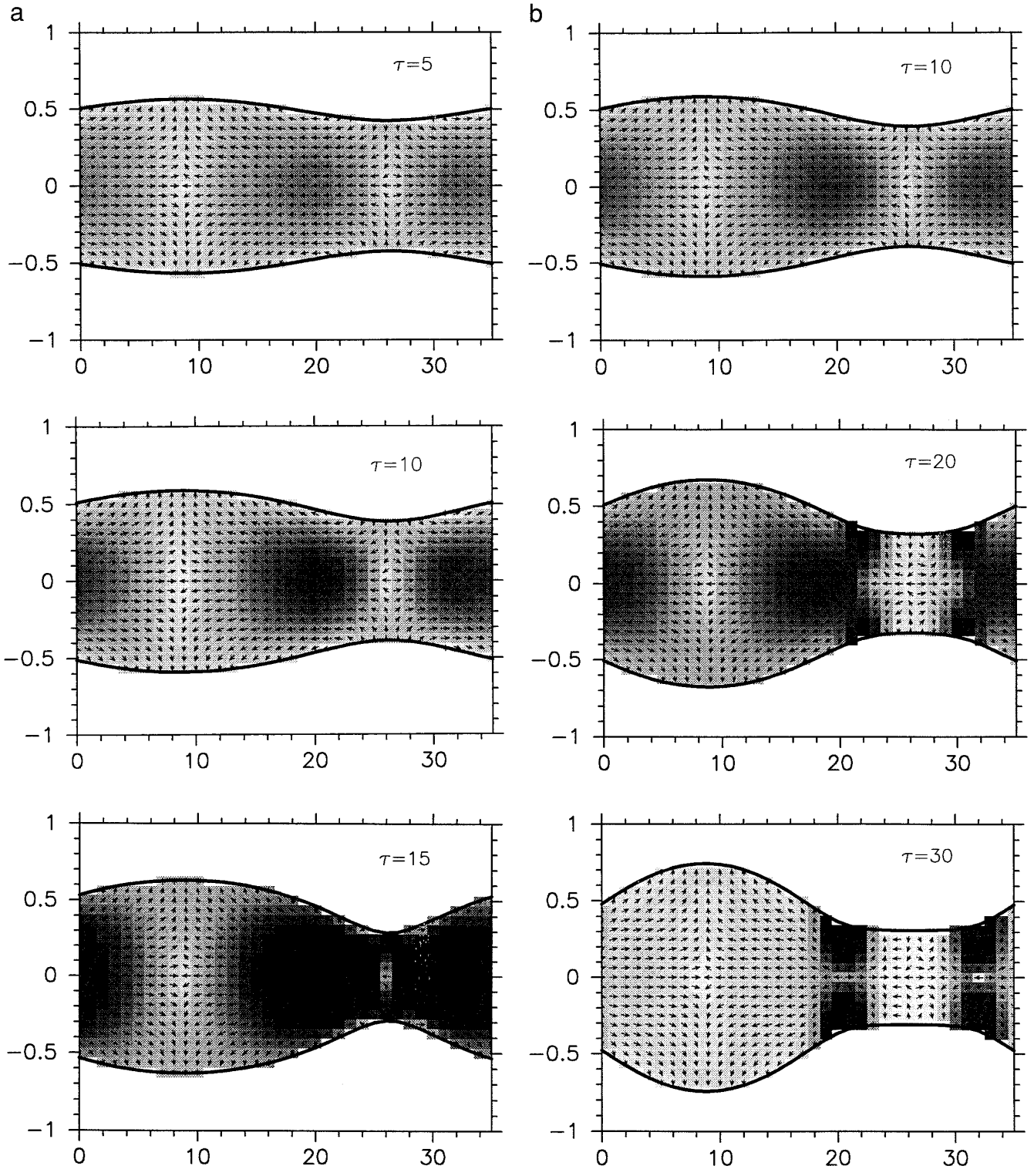

FIG. 6. Evolution of the velocity field inside the film for the same parametric values and initial conditions as in Figs. 3a and 3b, respectively. (a) Absence of either steric or electrostatic forces. (b) Presence of repulsive steric forces characterized by $\beta = 20$ and $p = 10^{-2}$. Each graph corresponds to the time indicated on the figure. At each grid site, an arrow indicates the direction of the velocity vector and a gray shade represents its intensity (increasing from white to black).

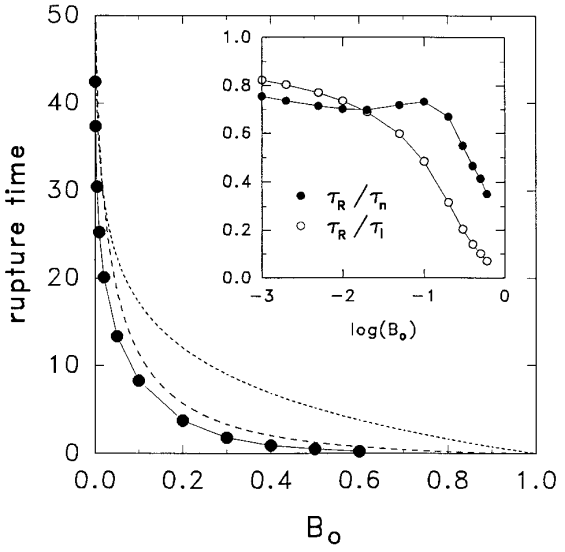

FIG. 7. Rupture time of a film subject to electric forces with $\alpha = 40$ and $q = 0.5$ as a function of the initial amplitude B_0. Steric forces were neglected. Short-dashed and dotted lines correspond, respectively, to the nonlinear and linear rupture times obtained from Eq. [23]; in the former case we assumed $\delta = \Delta = B_0/2$ and in the latter, $\Delta = 0$ and $\delta = B_0$. Symbols correspond to values obtained through numerical simulations. Insets: ratios τ_R/τ_l and τ_R/τ_n vs log B_0. Lines are guides to the eyes.

also verified numerically that for values of the wavenumber k above k_c, the perturbation vanishes.

5. DISCUSSION

A nonlinear evolution equation for the film thickness, Eq. [10], was obtained, at the long-wavelength approximation, through an electrohydrodynamical approach. Bulk phases are considered as incompressible viscous Newtonian fluids subject to van der Waals, steric, and electric bulk forces. We consider films with tangentially immobile surfaces and neglect lateral gradients of the surface tension and of the order parameter related to steric forces. Then, we obtain the governing equation [10]. Two electric cases are considered: (I) a film with equally charged surfaces and no potential drop, and (II) a neutral film under an external electric field. At the long-wave approximation, the film dynamics is not influenced by electric terms in case I. Nevertheless, in case II, a transmembrane potential influences film movement due to the discontinuity in the electric stress, even if the film has negligible surface charge. In fact, such electric discontinuity is a consequence of the difference of electric permittivity between the film phase and the external media. The electric term in Eq. [A20] holds for a transmembrane potential up to $4RT/Z_0$. Then, it is a good approximation for transmembrane potentials below 100 mV at temperatures of 25°C and below 150 mV at 37°C.

The nonlinear stability analysis was performed by linearizing the governing equation [10] around a nonhomogeneous stationary reference state while the linear analysis considers a planar state as the reference one. Consequently, the nonlinear approach preserves some nonlinear effects that are lost in the linear analysis. In the former, the growth rate, the cutoff wavenumber, and the fastest growth rate depend on the amplitude of the reference state Δ. As expected, the linear results are recovered for $\Delta = 0$.

The nonlinear approach shows that steric forces play a special role in the film dynamics that is not detectable in the linear analysis. For a given set of film parameters, the film can be either stable or unstable, depending on Δ (Fig. 2). There is a certain Δ_0 such that the perturbation either decreases if $\Delta > \Delta_0$ or increases if $\Delta < \Delta_0$. This results from the action of steric forces. Figure 2 shows that the fastest rate of growth ω_{nm} increases with Δ if steric forces are absent; however, if steric forces are operative ω_{nm} decreases from a certain value of Δ and vanishes for $\Delta = \Delta_0$. The nonlinear approach indicates that there exists a set of nonplanar stationary states for $\Delta > \Delta_0$. Indeed, numerical solution of the nonlinear governing equations indicates that, for a given set of the film parameters, the film evolves to a unique spatially nonhomogeneous steady state independent on the initial amplitude of the perturbation. Steric forces stabilize the film, delaying rupture as predicted by the linear and nonlinear approximations and also as already shown by other authors (8, 12); however, we also observed that strong steric forces prevent the film from narrowing beyond a minimum thickness. This numerical result, consistent with the predictions of the nonlinear stability analysis, could be interpreted as the increase of ordering of the hydrocarbon chains inside the film as its surfaces approach each other, due to the overlap of opposite chains. The linear analysis does not compute these nonlinear effects. Actually, the linear analysis

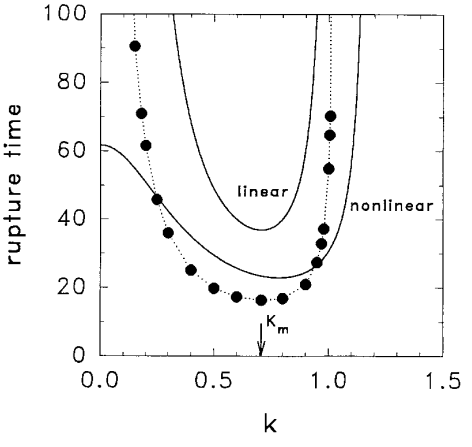

FIG. 8. Dependence of the rupture time on the wavenumber. The initial amplitude of the disturbance is $B_0 = 0.1$. Curves correspond to linear and nonlinear analytical values as indicated in the figure, and symbols correspond to values obtained through numerical integration.

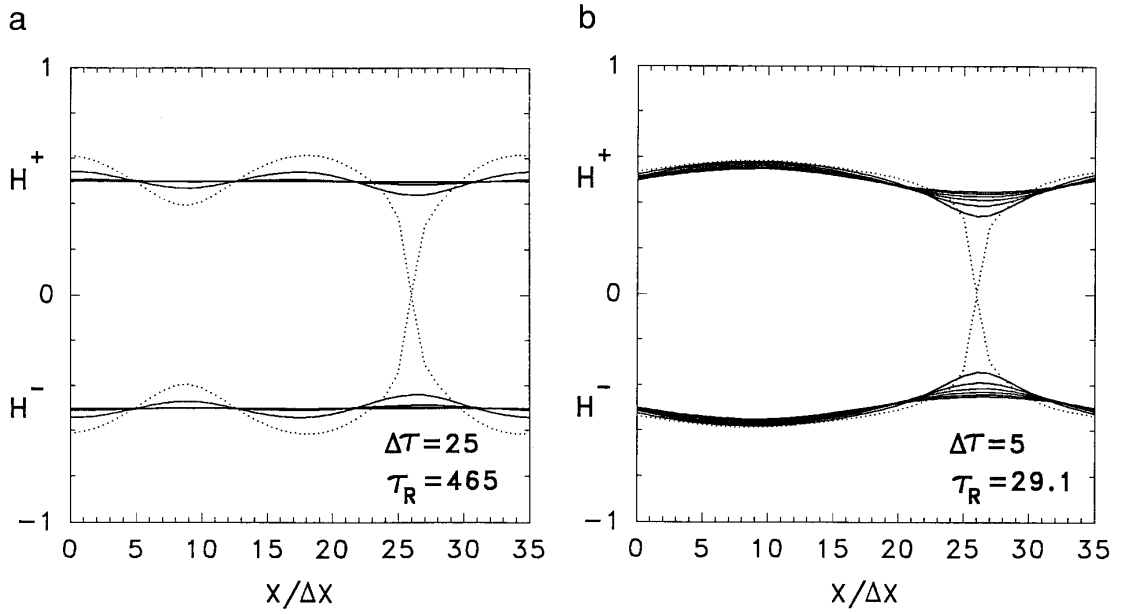

FIG. 9. Film surfaces described by $H^{\pm}(X, \tau) = \pm H(X, \tau)/2$ as a function of $X/\Delta X$, where the dimensionless thickness H was obtained following the nonlinear Eq. [10] and $\Delta X = 2\lambda_m/35$. Either steric or electrostatic forces are absent. In all cases the perturbation is in the $k_m/2$ mode. The perturbation initial amplitude is $B_0 = 10^{-7}$ (a) and 0.1 (b). Only one period of the periodic perturbation is represented. Rupture times τ_R and time intervals $\Delta\tau$ between plots are indicated on each figure. Dotted curves correspond to the last integration step preceding rupture. Numerical integrations were performed for time interval $\delta\tau = 5 \times 10^{-3}$.

investigates the stability of the planar state and it does not account for the increasing steric forces in the narrow regions of the deformed film. Thus, the linear approach underestimates steric effects. Moreover, both from the nonlinear approach and from numerical results, the values of p and β allowing film rupture correspond to $\frac{1}{2}A_{\beta'}\beta'^2\eta_s^2 \approx 10^{12}$ dyn/cm^2 and $\beta'^{-1} \approx 2.3 \times 10^{-8}$ cm, which are in the range of the smallest values usually adopted for the steric parameters (10^{12} dyn/cm$^2 \leqslant \frac{1}{2}A_{\beta'}\beta'^2\eta_s^2 \leqslant 10^{15}$ dyn/cm^2 and 2.1×10^{-8} cm $\leqslant \beta'^{-1} \leqslant 3.4 \times 10^{-8}$ cm) (12). For larger values of the steric parameters, the film is stable and it does not break even when subject to van der Waals forces and electric forces derived from a potential drop of order of 100 mV.

In case II, electric destabilizing forces are operative due to a transmembrane potential that results in a nonvanishing electric field both inside the film and in the external bulk phases. Discontinuity of electric stress across the interfaces contributes to film destabilization. For a given transmembrane potential, electric destabilizing effects increase with the electrolytic concentration in the bulk external phases. Since electric forces act as destabilizing ones, an initially stable film can become unstable if electric forces are large enough to counterbalance steric repulsive forces. It is shown that transmembrane potentials up to 150 mV do not affect film stability; however, the approximation taken into account for the electric term does not hold for values of the potential drop that could lead the film to rupture. From Fig. 5a, showing the dependence of rupture time on parameter $q \propto (\Delta\psi_T)^2$, we note that an increase in the transmembrane potential accelerates rupture. From this result one can infer that membrane rupture may be induced by an electric signal that originates a potential drop across the film. Indeed, a procedure commonly used to insert foreign material into the cell is electropermeabilization (27, 28). When an electrical potential of order 1 V is induced across a cell membrane for a fraction of a second, membrane permeability increases drastically, leading to leakage or uptake of molecules normally excluded from membrane transport. As a special case, actual pores may be formed (electroporation). The present model cannot predict whether actual pores are formed. The extension of the model to three dimensions could elucidate that point. Even if charge densities are negligible, the electric stress due to the dielectric discontinuity at the film surfaces yields film deformation leading to rupture. Salt effects are expressed through the parameter α, inversely related to the Debye length. The destabilizing effect of electrostatic forces becomes stronger as α increases. In fact, if salt concentration increases, the Debye length decreases (hence, α increases) and the potential drop across the film ($\Delta\psi_0$) grows closer to the transmembrane potential $\Delta\psi_T$, therefore increasing the electric stress. Taking into account the approximate relation $\Delta\psi_0 = [\alpha H/(1 + \alpha H)]\Delta\psi_T$, note that as H decreases, $\Delta\psi_0$ also decreases. Then, the electric destabilizing effect is reduced as the film approaches rupture.

From the choice of the relationship $\Delta = \delta$ it is shown that nonlinearities accelerate film rupture. Nonlinear rupture time can be up to 10 times lower than linear rupture time (Fig. 8). For film parameters corresponding to Fig. 8, $B_0 = 0.5$ and $\Sigma = 5$ dyn/cm^2, the linear and nonlinear rupture times approach, respectively, 140 and 476 ms. Indeed, numerical results show that nonlinearities accelerate film rupture more strongly than indicated by the nonlinear approach, and in that case the numerically computed rupture time approximates 25 msec. In fact, the nonlinear stability analysis developed here does not allow us to follow completely the film movement until film rupture; however, beyond calculation of the rupture time, the nonlinear approach helps us to understand the role of nonlinearities in film dynamics.

The evolution of a perturbation is highly dependent on initial amplitudes and wavenumbers. Thus, when dealing with actual disturbances originated either by some driving force inducing the perturbation or by spontaneous fluctuations due to thermal noise, and normally composed by a set of interacting modes, it is necessary to know the whole initial spectrum to follow correctly the evolution of the surface deformation. Here, we investigated the dynamics of the rupture and its dependence on the different forces acting on the system when the film is perturbed in the k_m SQ mode which is expected to dominate the evolution. Observe from Fig. 9 that the k_m mode develops even when it is absent in the initial wave.

Analytical approximations give a clue to the qualitative effect of the different interactions on the rupture time; however, they apply to situations characterized by initially small-amplitude disturbances from the planar state. As depicted in Fig. 7, although the nonlinear approach yields results closer to the numerical ones, both analytical approximations lead to overestimation of the rupture time relative to the numerically obtained one. Therefore, rupture times depend strongly on the nonlinearities of the problem.

APPENDIX

To solve the nonlinear hydrodynamic problem we put all the equations in a dimensionless form (3, 12, 13, 29) using the Stokes scale $x' = x/h_0$, $z' = z/h_0$, and $t' = \nu t/h_0^2$, where h_0 is the mean film thickness and $\nu = \mu/\rho$ is the kinematic viscosity. Instabilities are expected for perturbations with wavelength $\lambda \gg h_0$ (1, 14–17). Then, we rescale again the equations and boundary conditions introducing a small parameter $\theta = h_0/\lambda$ appropriate for the long-wavelength approximation, and the total scaling reads

$$\tilde{x} = \theta \frac{x}{h_0}, \quad \tilde{z} = \frac{z}{h_0}, \quad \tilde{t} = \theta \frac{\nu t}{h_0^2}, \quad \tilde{h} = \frac{h}{h_0},$$
$$\tilde{u} = \frac{h_0 u}{\nu}, \quad \tilde{v} = \theta^{-1} \frac{h_0 v}{\nu}, \quad \tilde{p} = \theta \frac{h_0^2 p}{\rho \nu^2}. \qquad [A1]$$

We develop each quantity in regular expansion in the form

$$(\tilde{u}, \tilde{v}, \tilde{p}) = \sum_{n=0}^{\infty} \theta^n (\tilde{u}_n, \tilde{v}_n, \tilde{p}_n). \qquad [A2]$$

To obtain an approximate solution of the problem we have taken all the nondimensional equations and boundary conditions at zero order of θ. In this case, the x and z components of the Navier–Stokes equation [1] read, respectively,

$$\left[\tilde{p} - \tilde{\phi} - \frac{\epsilon - 1}{2} \tilde{\psi}_{\tilde{z}}^2 - 8\pi \tilde{C}_0 \tilde{R}\tilde{T} \cosh\left(\frac{\tilde{Z}_0 \tilde{\psi}}{\tilde{R}\tilde{T}} \right) + \tilde{W} \right]_{\tilde{x}} = r \tilde{u}_{\tilde{z}\tilde{z}} \qquad [A3]$$

and

$$\left[\tilde{p} - \tilde{\phi} - \frac{\epsilon - 1}{2} \tilde{\psi}_{\tilde{z}}^2 - 8\pi \tilde{C}_0 \tilde{R}\tilde{T} \cosh\left(\frac{\tilde{Z}_0 \tilde{\psi}}{\tilde{R}\tilde{T}} \right) + \tilde{W} \right]_{\tilde{z}} = 0, \qquad [A4]$$

where we have used the Poisson–Boltzmann equation [5]. The subscripts $\tilde{x}$ and $\tilde{z}$ indicate partial derivatives and $r = \nu'/\nu$. In the internal phase, $r = 1$ and the hyperbolic term vanishes as there is no net electric charge. Otherwise, at the external bulk phases the steric potential ϕ vanishes since hydrocarbon chains are absent.

We have conveniently estimated each physical quantity responsible for the film instability to preserve the corresponding terms comparable to the viscous term at zero order. Then, we take

$$\tilde{\phi} = \theta \frac{h_0^2 \psi}{\rho \nu^2}, \quad \tilde{\psi} = \left(\frac{\theta}{4\pi \rho \nu^2} \right)^{1/2} \psi, \quad \tilde{C}_0 = h_0^3 C_0,$$
$$\tilde{Z}_0 = \left(\frac{\theta}{4\pi \rho' \nu^2 h_0^2} \right)^{1/2} Z_0, \quad \tilde{R}\tilde{T} = \frac{\theta}{4\pi \rho' \nu^2 h_0} RT,$$
$$\text{and} \quad \tilde{W} = \theta \frac{h_0^2}{\nu^2} W. \qquad [A5]$$

At the long-wavelength limit, the incompressibility condition [2] reads

$$\tilde{v}_{\tilde{x}} + \tilde{v}_{\tilde{z}} = 0. \qquad [A6]$$

For the Laplace [4] and Poisson–Boltzmann [5] equations, we have, respectively,

$$\tilde{\phi}_{\tilde{z}\tilde{z}} = 0 \qquad [A7]$$

and

$$\tilde{\phi}'_{\tilde{z}\tilde{z}} = \frac{8\pi\tilde{Z}_0\tilde{C}_0}{\epsilon'}\sinh\left(\frac{\tilde{Z}_0\tilde{\psi}}{\tilde{R}\tilde{T}}\right). \quad [A8]$$

Thus, in the long-wavelength approximation these equations are second-order partial derivative equations in z only. At the interfaces, we considered the boundary conditions at zero order derived from the normal momentum balance (Eq. [6]) for nonviscous surfaces, the electric displacement condition (Eq. [7]), the electric potential condition (Eq. [8]), and the equation for the order parameter (12).

Since we consider a film in the SQ mode, the normal velocity components are antisymmetric and the tangential ones are symmetric (3). Moreover, we assume the continuity of the velocity field across the interfaces (3). Finally, we considered the adimensional form of the kinematic condition Eq. [9] at the long-wavelength limit. These conditions allow us to integrate the x component of the Navier–Stokes equation [A3] and to obtain the components of the tangential velocity of the fluid elements. Then, we obtain the normal components of the velocity by integrating the continuity equation [A6] and using the SQ mode boundary conditions. The substitution of the velocity components in the kinematic condition [9] gives us the spatiotemporal nonlinear film thickness evolution equation for a symmetric film:

$$\frac{1}{2}\tilde{h}_{\tilde{t}} + \frac{1}{3}\left\{\left(\frac{\tilde{h}}{2}\right)^3\left[3\tilde{S}\tilde{h}_{\tilde{x}\tilde{x}} + 2\tilde{\phi} - \frac{\tilde{\phi}_{\tilde{z}\tilde{z}}}{2\beta^2} - \frac{\epsilon}{2}\tilde{\psi}_{\tilde{z}}^2 + \frac{\rho'}{\rho}\frac{\epsilon'}{2}\tilde{\psi}_{\tilde{z}}'^2 - 8\pi\frac{\rho'}{\rho}\tilde{C}_0\tilde{R}\tilde{T}\cosh\left(\frac{\tilde{Z}_0\tilde{\psi}}{\tilde{R}\tilde{T}}\right) - \tilde{W} + \frac{\rho'}{\rho}\tilde{W}'\right]_{\tilde{x}}\right\}_{\tilde{x}} = 0. \quad [A9]$$

$\tilde{S} = \theta^3(h_0/3\rho\nu^2)\Sigma$ is the inverse of the capillarity number and $\beta = \beta' h_0$, where $1/\beta'$ measures the interaction range between oriented hydrocarbon chains [8].

Equation [10] is a nonlinear equation for the film thickness evolution at the long-wavelength approximation. To solve it, we need to find the surface tension and the bulk force potentials as functions of $h(x, t)$. We consider a film with tangentially immobile surfaces in which there is no lateral gradient of surface tension, that is, $\tilde{\Sigma}_{\tilde{x}} = 0$.

The steric and van der Waals terms were obtained previously (12). The electric potential into the film satisfies the Laplace equation [4] and is given by the expression

$$\tilde{\psi} = \Delta\tilde{\psi}\frac{\tilde{z}}{\tilde{h}} + \frac{\tilde{\psi}_1 + \tilde{\psi}_2}{2}, \quad [A10]$$

where $\Delta\tilde{\psi} = \tilde{\psi}_1 - \tilde{\psi}_2$ is the transbilayer potential, i.e., the potential difference between S_1 and S_2. The solution of the Poisson–Boltzmann equation [5] at the long-wave approximation gives the electric potential at the external phases P_1 and P_3,

$$\tilde{\psi}' = \tilde{\psi}'_{\mp\infty} \mp \frac{2\tilde{R}\tilde{T}}{\tilde{Z}_0}\frac{1 + \mathrm{tgh}\left(\frac{\tilde{Z}_0\Delta\tilde{\psi}'}{4\tilde{R}\tilde{T}}\right)\exp[\pm\tilde{\chi}(\tilde{z} \pm \tilde{h}/2)]}{1 - \mathrm{tgh}\left(\frac{\tilde{Z}_0\Delta\tilde{\psi}'}{4\tilde{R}\tilde{T}}\right)\exp[\pm\tilde{\chi}(\tilde{z} \pm \tilde{h}/2)]}, \quad [A11]$$

where $\tilde{\chi} = (8\pi\tilde{Z}_0^2\tilde{C}_0/\epsilon'\tilde{R}\tilde{T})^{1/2}$is the dimensionless inverse of the Debye length. The plus–minus signs in Eq. [A11] account, respectively, for phases P_1 (upper) and P_3 (down), and $\Delta\tilde{\psi}' = \Delta\tilde{\psi}'_1 = \tilde{\psi}'_{-\infty} - \tilde{\psi}'_1$ in P_1 while $\Delta\tilde{\psi}' = \Delta\tilde{\psi}'_3 = \tilde{\psi}'_2 - \tilde{\psi}'_{+\infty}$ in P_3.

From Eqs. [A10] and [A11], the remaining electric term in Eq. [A9] is

$$-\frac{\epsilon}{2}\tilde{\psi}_{\tilde{z}}^2 + \frac{\rho'}{\rho}\frac{\epsilon'}{2}\tilde{\psi}_{\tilde{z}}'^2 - 8\pi\frac{\rho'}{\rho}\tilde{C}_0\tilde{R}\tilde{T}\cosh\left(\frac{\tilde{Z}_0\tilde{\psi}}{\tilde{R}\tilde{T}}\right) = -\frac{\epsilon}{2}\left(\frac{\Delta\tilde{\psi}}{\tilde{h}}\right)^2. \quad [A12]$$

In agreement with the continuity of the potential across the interfaces [8], the potential difference across the whole system (transmembrane potential, $\Delta\tilde{\psi}_T$) is

$$\Delta\tilde{\psi}_T = \tilde{\psi}'_{-\infty} - \tilde{\psi}'_{+\infty} = \Delta\tilde{\psi}'_1 + \Delta\tilde{\psi} + \Delta\tilde{\psi}'_3. \quad [A13]$$

Substituting Eqs. [A10] and [A11] into Eq. [7], we have the following conditions at interfaces S_1 and S_2, respectively:

$$\frac{2\tilde{R}\tilde{T}\chi\epsilon'}{\tilde{Z}_0}\sinh\left(\frac{\tilde{Z}_0\Delta\tilde{\psi}'_1}{2\tilde{R}\tilde{T}}\right) - \epsilon\frac{\Delta\tilde{\psi}}{\tilde{h}} = -4\pi\sigma_1,$$

$$\frac{2\tilde{R}\tilde{T}\chi\epsilon'}{\tilde{Z}_0}\sinh\left(\frac{\tilde{Z}_0\Delta\tilde{\psi}'_3}{2\tilde{R}\tilde{T}}\right) - \epsilon\frac{\Delta\tilde{\psi}}{\tilde{h}} = 4\pi\sigma_2. \quad [A14]$$

Here σ_1 and σ_2 are the surface charge densities on S_1 and S_2, respectively.

For case I, a film with equally charged surfaces and $\Delta\tilde{\psi}_T = \Delta\tilde{\psi} = 0$, one gets from Eqs. [A14] that $\Delta\tilde{\psi}'_1 = -\Delta\tilde{\psi}'_3$. These considerations lead to the evolution equation

$$H_\tau + \frac{1}{4}\left[H^3 H_{XXX} + H^{-1}H_X - \mathrm{P}\,\frac{\sinh(\beta H/2)}{\cosh^3(\beta H/2)}\,H^3 H_X\right]_X = 0, \quad [A15]$$

where we have defined new variables for space and time,

$$X = (\tilde{A}/\tilde{S})^{1/2}\tilde{x}, \quad H = \tilde{h}, \quad \tau = (\tilde{A}^2/\tilde{S})\tilde{t}, \quad [A16]$$

and the nondimensional parameter

$$P = \frac{\tilde{A}_\beta \tilde{\beta}^3 \tilde{\eta}_s^2}{6\tilde{A}}, \quad [A17]$$

with $\tilde{A}_\beta = A_\beta/\rho\nu^2 h_0^4$ and $\tilde{A} = \theta A/6\pi\rho\nu^2 h_0^2$, where A is the Hamaker constant.

Equation [A15] shows that in case I there are no electric effects on the film evolution at the long-wave approximation, consistent with the results obtained from linear analysis (30).

For case II, a neutral film submitted to an external constant electric field, one obtains from Eqs. [A14] that $\Delta\tilde{\psi}_1' = \Delta\tilde{\psi}_3'$. Then, Eqs. [A13] and [A14] yield

$$\epsilon\,\frac{\Delta\tilde{\psi}}{\tilde{h}} = \frac{2\tilde{R}\tilde{T}\chi\epsilon'}{\tilde{Z}_0}\sinh\left(\frac{\tilde{Z}_0(\Delta\tilde{\psi}_\mathrm{T} - \Delta\tilde{\psi})}{4\tilde{R}\tilde{T}}\right). \quad [A18]$$

For $\tilde{Z}_0\Delta\tilde{\psi}_\mathrm{T}/4\tilde{R}\tilde{T} \leqslant 1$, Eq. [A18] leads to the approximation

$$\frac{\Delta\tilde{\psi}}{\tilde{h}} = \frac{\alpha\Delta\tilde{\psi}_\mathrm{T}}{1 + \alpha\tilde{h}}. \quad [A19]$$

At ca. 25°C, Eq. [A19] is a good approximation for $\Delta\psi_\mathrm{T} \leqslant 100$ mV. Then, from Eqs. [A9], [A12], and [A19], the evolution equation for case II reads

$$H_\tau + \frac{1}{4}\left[H^3 H_{XXX} + H^{-1}H_X - \mathrm{P}\,\frac{\sinh(\beta H/2)}{\cosh^3(\beta H/2)}\,H^3 H_X + \mathrm{q}\left(\frac{\alpha H}{1 + \alpha H}\right)^3 H_X\right]_X = 0, \quad [A20]$$

where we defined the nondimensional parameters

$$q = \frac{\epsilon(\Delta\tilde{\psi}_\mathrm{T})^2}{3\tilde{A}}, \qquad \alpha = \frac{\epsilon'\chi h_0}{2\epsilon}, \quad [A21]$$

where χ is the inverse of the Debye length.

It is also interesting to know the evolution of the velocity field inside the film. At the long-wavelength limit, the dimensionless expressions at zero order for the tangential ($\tilde{u}$) and normal ($\tilde{v}$) velocities may be obtained as functions of the dimensionless spatial coordinates and time:

$$\tilde{u}(X, Z, \tau) = -(Z^2 - (H/2)^2)f/2, \quad [A22]$$

$$\tilde{v}(X, Z, \tau) = ((Z^2/3 - (H/2)^2)f_X - (H/2)fH_X)Z/2, \quad [A23]$$

with

$$f = s\left(H_{XXX} + H^{-4}H_X - P\,\frac{\sinh(\beta H/2)}{\cosh^3(\beta H/2)}\,H_X + \mathrm{q}\left(\frac{\alpha}{1 + \alpha H}\right)^3 H_X\right), \quad [A24]$$

where $Z = z/h_0$ is the dimensionless coordinate normal to the symmetry plane and $s = 3(\tilde{A}^3/\tilde{S})^{1/2}$.

ACKNOWLEDGMENTS

We acknowledge Professor D. Gallez, Université Libre de Bruxelles, for some advice on numerical computation. We also thank Brazilian agencies CNPq and Capes for financial support.

REFERENCES

1. Singer, S. J., and Nicholson, G. L., *Science* **175,** 720 (1972).
2. Gallez, D., and Coackley, W. T., *Prog. Biophys. Mol. Biol.* **48,** 155 (1986).
3. Williams, M. B., and Davies, S. H., *J. Colloid Interface Sci.* **90,** 220 (1982).
4. Sharma, A., and Ruckenstein, E., *J. Colloid Interface Sci.* **113,** 456 (1986).
5. Sharma, A., and Ruckenstein, E., *AIChE Symp. Ser.* **82,** 123 (1986).
6. Sharma, A., and Ruckenstein, E., *AIChE Symp. Ser.* **82,** 129 (1986).
7. Felderhof, B. U., *J. Chem. Phys.* **49**(1), 44 (1968).
8. Bisch, P. M., and Wendel, H., *J. Chem. Phys.* **83,** 5953 (1985).
9. Aris, R., ''Vectors, Tensors and the Basic Equations of Fluid Mechanics. Dover, New York, 1989.
10. Mitlin, V. S., *J. Colloid Interface Sci.* **156,** 491 (1993).
11. Sharma, A., and Jarneel, A. T., *J. Colloid Interface Sci.* **161,** 190 (1993).
12. Gallez, D., Costa Pinto, N. M., and Bisch, P. M., *J. Colloid Interface Sci.* **160,** 141 (1993).
13. Prévost, M., and Gallez, D., *J. Chem. Phys.* **84,** 4043 (1986).
14. Fettiplace, R., Gordon, L. G. M., Hiladky, S. B., Requena, J., Zingsheim, H. P., and Haydon, D. A., *in* ''Methods in Membrane Biology,'' Vol. 4, p. 1. Plenum, New York, 1974.
15. Benz, R., Frölich, O., Läuger, P., and Montal, M., *Biochim. Biophys. Acta* **394,** 323 (1975).
16. Fisher, L. R., and Parker, N. S., *Biophys. J.* **46,** 253 (1984).

17. Leihler, S., *J. Phys.* **47,** 507 (1986).
18. Läuger, P., Lesslauer, W., Marte, E., and Richter, J., *Biochim. Biophys. Acta* **135,** 20 (1967).
19. Nir, S., and Bentz, J., *J. Colloid Interface Sci.* **65,** 399 (1978).
20. Bisch, P. M., Wendel, H., and Gallez, D., *J. Colloid Interface Sci.* **92,** 105 (1983).
21. Wendel, H., Bisch, P. M., and Gallez, D., *Colloid Polymer Sci.* **260,** 425 (1982).
22. Gallez, D., *Biophys. Chem.* **18,** 165 (1983).
23. Gallez, D., Privost, M., and Sanfeld, A., *Colloids Surf.* **10,** 123 (1984).
24. Horn, R. G., *Biochim. Biophys. Acta* **778,** 224 (1984).
25. Helm, C. A., Israelachvilli, N., and McGuiggan, P. M., *Science* **246,** 919 (1989).
26. Press, W. H., Teukolsky, S. A., Vetterling, W. T., and Flannery, ''Numerical Recipes in Fortran: The Art of Scientific Computing.'' Cambridge Univ. Press, London/New York, 1992.
27. Tsong, T. Y., *Biophys. J.* **60,** 297–301 (1991).
28. Ghosh, P. M., Keese, C. R., and Giaever, I., *Biophys. J.* **64,** 1602 (1993).
29. De Wit, A., Gallez, D., and Christov, C. I., *Phys. Fluids* **6,** 3256 (1994).
30. Bisch, P. M., ''On the Electrochemical Hydrodynamics of Fluid Interfaces: Stability and Surface Waves.'' Thèse de Docteur, Université Libre de Bruxelles, 1980.